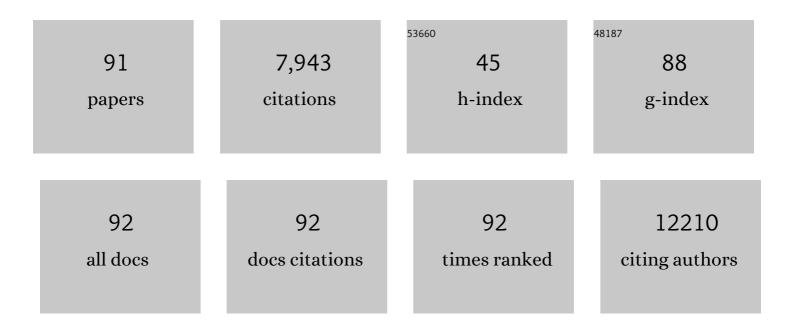
## List of Publications by Year in descending order

Source: https://exaly.com/author-pdf/132978/publications.pdf Version: 2024-02-01



Ητιλ Χτι

#	Article	IF	CITATIONS
1	Airâ€Stable 2D Cr <sub>5</sub> Te <sub>8</sub> Nanosheets with Thicknessâ€Tunable Ferromagnetism. Advanced Materials, 2022, 34, e2107512.	11.1	77
2	Polarization Sensitive Solarâ€Blind Ultraviolet Photodetectors Based on Ultrawide Bandgap KNb <sub>3</sub> O <sub>8</sub> Nanobelt with Fringe‣ike Atomic Lattice. Advanced Functional Materials, 2022, 32, .	7.8	41
3	Fast Identification of the Crystallographic Orientation of Violet Phosphorus Nanoflakes with Preferred Inâ€Plane Cleavage Edge Orientation. Advanced Functional Materials, 2022, 32, .	7.8	24
4	Multiple 2D Phase Transformations in Monolayer Transition Metal Chalcogenides. Advanced Materials, 2022, 34, e2200643.	11.1	6
5	Improving Harsh Environmental Stability of Few‣ayer Black Phosphorus by Local Charge Transfer. Advanced Functional Materials, 2022, 32, .	7.8	11
6	Electrochemical Delamination of Ultralarge Few‣ayer Black Phosphorus with a Hydrogenâ€Free Intercalation Mechanism. Advanced Materials, 2021, 33, e2005815.	11.1	22
7	Deciphering the Intense Postgap Absorptions of Monolayer Transition Metal Dichalcogenides. ACS Nano, 2021, 15, 7783-7789.	7.3	4
8	Realizing the Intrinsic Anisotropic Growth of 1T′ ReS <sub>2</sub> on Selected Au(101) Substrate toward Large cale Single Crystal Fabrication. Advanced Functional Materials, 2021, 31, 2102138.	7.8	27
9	Controllable growth of typeâ€I Dirac semimetal PtTe <sub>2</sub> atomic layer on Au substrate for sensitive room temperature terahertz photodetection. InformaÄnÃ-Materiály, 2021, 3, 705-715.	8.5	33
10	Synthesis of Large-Area Uniform MoS <sub>2</sub> –WS <sub>2</sub> Lateral Heterojunction Nanosheets for Photodetectors. ACS Applied Nano Materials, 2021, 4, 5522-5530.	2.4	17
11	Probing Atomicâ€Scale Fracture of Grain Boundaries in Lowâ€symmetry 2D Materials. Small, 2021, 17, e2102739.	5.2	7
12	Insight into the Role of H <sub>2</sub> in WS <sub>2</sub> Growth by Chemical Vapor Deposition. ACS Applied Electronic Materials, 2021, 3, 5138-5146.	2.0	5
13	2H/1T′ phase WS2(1â~'x)Te2x alloys grown by chemical vapor deposition with tunable band structures. Applied Surface Science, 2020, 504, 144371.	3.1	18
14	Atomic-Scale Studies of Overlapping Grain Boundaries between Parallel and Quasi-Parallel Grains in Low-Symmetry Monolayer ReS2. Matter, 2020, 3, 2108-2123.	5.0	11
15	2D Reâ€Based Transition Metal Chalcogenides: Progress, Challenges, and Opportunities. Advanced Science, 2020, 7, 2002320.	5.6	62
16	Strong Band Bowing Effects and Distinctive Optoelectronic Properties of 2H and 1T′ Phaseâ€īunable Mo <i><sub>x</sub></i> Re <sub>1–</sub> <i><sub>x</sub></i> S <sub>2</sub> Alloys. Advanced Functional Materials, 2020, 30, 2003264.	7.8	39
17	STEM imaging artifacts with three-fold astigmatism in monolayer transition metal dichalcogenides. Applied Physics Letters, 2020, 116, .	1.5	5
18	Epitaxial Growth of Rectangle Shape MoS <sub>2</sub> with Highly Aligned Orientation on Twofold Symmetry aâ€Plane Sapphire. Small, 2020, 16, e2000596.	5.2	53

#	Article	IF	CITATIONS
19	Synthesis of 2Hâ€IT′ WS <sub>2</sub> â€ReS <sub>2</sub> Heterophase Structures with Atomically Sharp Interface via Hydrogenâ€Triggered Oneâ€Pot Growth. Advanced Functional Materials, 2020, 30, 1910169.	7.8	42
20	Seismic risk evaluation for a planning mountain tunnel using improved analytical hierarchy process based on extension theory. Journal of Mountain Science, 2020, 17, 244-260.	0.8	13
21	Low-temperature growth of Three dimensional ReS2/ReO2 metal-semiconductor heterojunctions on Graphene/polyimide film for enhanced hydrogen evolution reaction. Applied Catalysis B: Environmental, 2020, 271, 118924.	10.8	28
22	Linear Dichroism and Nondestructive Crystalline Identification of Anisotropic Semimetal Few‣ayer MoTe <sub>2</sub> . Small, 2019, 15, e1903159.	5.2	24
23	2D MoTe <sub>2</sub> : Linear Dichroism and Nondestructive Crystalline Identification of Anisotropic Semimetal Few‣ayer MoTe <sub>2</sub> (Small 44/2019). Small, 2019, 15, 1970239.	5.2	1
24	Nanoassembly Growth Model for Subdomain and Grain Boundary Formation in 1T′ Layered ReS <sub>2</sub> . Advanced Functional Materials, 2019, 29, 1906385.	7.8	45
25	Evaluation of Ground Surface Pregrouting in a Mountain Tunnel Based on FAHP. Mathematical Problems in Engineering, 2019, 2019, 1-17.	0.6	1
26	Chemical Vapor Deposition Growth of High Crystallinity Sb <sub>2</sub> Se <sub>3</sub> Nanowire with Strong Anisotropy for Nearâ€Infrared Photodetectors. Small, 2019, 15, e1805307.	5.2	93
27	Fe <sub>3</sub> O <sub>4</sub> nanoparticles as a saturable absorber for giant chirped pulse generation. Beilstein Journal of Nanotechnology, 2019, 10, 1065-1072.	1.5	18
28	Doping modulated in-plane anisotropic Raman enhancement on layered ReS2. Nano Research, 2019, 12, 563-568.	5.8	15
29	Spatially Confined Growth of Fullerene to Superâ€Long Crystalline Fibers in Supramolecular Gels for Highâ€Performance Photodetector. Advanced Materials, 2019, 31, e1808254.	11.1	42
30	Intercalation and delamination behavior of Ti <sub>3</sub> C <sub>2</sub> T <sub>x</sub> and MnO <sub>2</sub> /Ti <sub>3</sub> C <sub>2</sub> T <sub>x</sub> /RGO flexible fibers with high volumetric capacitance. Journal of Materials Chemistry A, 2019, 7, 12582-12592.	5.2	48
31	Grain Boundaries: Nanoassembly Growth Model for Subdomain and Grain Boundary Formation in 1T′ Layered ReS <sub>2</sub> (Adv. Funct. Mater. 49/2019). Advanced Functional Materials, 2019, 29, 1970335.	7.8	1
32	Highly Compressible Carbon Sponge Supercapacitor Electrode with Enhanced Performance by Growing Nickel–Cobalt Sulfide Nanosheets. ACS Applied Materials & Interfaces, 2018, 10, 10087-10095.	4.0	111
33	Electrostatic Functionalization and Passivation of Water-Exfoliated Few-Layer Black Phosphorus by Poly Dimethyldiallyl Ammonium Chloride and Its Ultrafast Laser Application. ACS Applied Materials & Interfaces, 2018, 10, 9679-9687.	4.0	57
34	Thermodynamics and Kinetics Synergetic Phase-Engineering of Chemical Vapor Deposition Grown Single Crystal MoTe <sub>2</sub> Nanosheets. Crystal Growth and Design, 2018, 18, 2844-2850.	1.4	22
35	2D Layered Materialâ€Based van der Waals Heterostructures for Optoelectronics. Advanced Functional Materials, 2018, 28, 1706587.	7.8	279
36	Block poly(arylene ether sulfone) copolymers tethering aromatic side-chain quaternary ammonium as anion exchange membranes. Polymer Chemistry, 2018, 9, 699-711.	1.9	46

#	Article	IF	CITATIONS
37	Spotting the differences in two-dimensional materials – the Raman scattering perspective. Chemical Society Reviews, 2018, 47, 3217-3240.	18.7	71
38	Investigation of black phosphorus as a nano-optical polarization element by polarized Raman spectroscopy. Nano Research, 2018, 11, 3154-3163.	5.8	19
39	Multi-inch single-crystalline perovskite membrane for high-detectivity flexible photosensors. Nature Communications, 2018, 9, 5302.	5.8	212
40	Nb <sub>2</sub> O <sub>5</sub> Nanoparticles Anchored on an N-Doped Graphene Hybrid Anode for a Sodium-Ion Capacitor with High Energy Density. ACS Omega, 2018, 3, 15943-15951.	1.6	30
41	Diverse Atomically Sharp Interfaces and Linear Dichroism of 1T' ReS <sub>2</sub> â€ReSe <sub>2</sub> Lateral p–n Heterojunctions. Advanced Functional Materials, 2018, 28, 1804696.	7.8	50
42	Metallic-Phase MoS <sub>2</sub> Nanopetals with Enhanced Electrocatalytic Activity for Hydrogen Evolution. ACS Sustainable Chemistry and Engineering, 2018, 6, 13435-13442.	3.2	48
43	CoNi <sub>2</sub> S <sub>4</sub> Nanoparticle/Carbon Nanotube Sponge Cathode with Ultrahigh Capacitance for Highly Compressible Asymmetric Supercapacitor. Small, 2018, 14, e1800998.	5.2	87
44	Rational design and controllable preparation of holey MnO <sub>2</sub> nanosheets. Chemical Communications, 2017, 53, 2950-2953.	2.2	18
45	Photothermal Catalysis: Targeting Activation of CO <sub>2</sub> and H <sub>2</sub> over Ruâ€Loaded Ultrathin Layered Double Hydroxides to Achieve Efficient Photothermal CO <sub>2</sub> Methanation in Flowâ€Type System (Adv. Energy Mater. 5/2017). Advanced Energy Materials, 2017, 7, .	10.2	5
46	Chemical Vapor Deposition Growth of Linked Carbon Monolayers with Acetylenic Scaffoldings on Silver Foil. Advanced Materials, 2017, 29, 1604665.	11.1	114
47	Highly flexible all-solid-state cable-type supercapacitors based on Cu/reduced graphene oxide/manganese dioxide fibers. RSC Advances, 2017, 7, 10092-10099.	1.7	25
48	Epitaxial growth of large-area and highly crystalline anisotropic ReSe2 atomic layer. Nano Research, 2017, 10, 2732-2742.	5.8	69
49	Solution Coating of Superior Largeâ€Area Flexible Perovskite Thin Films with Controlled Crystal Packing. Advanced Optical Materials, 2017, 5, 1700102.	3.6	34
50	Synthesis of Large‧ize 1T′ ReS <sub>2</sub> <i><sub>x</sub></i> Se <sub>2(1â^'</sub> <i><sub>x</sub></i> <sub>)</sub> Alloy Monolayer with Tunable Bandgap and Carrier Type. Advanced Materials, 2017, 29, 1705015.	11.1	107
51	Cellular Architectureâ€Based Allâ€Polymer Flexible Thinâ€Film Photodetectors with High Performance and Stability in Harsh Environment. Advanced Materials Technologies, 2017, 2, 1700185.	3.0	7
52	Characteristics and applications of ecological soil substrate for rocky slope vegetation in cold and high-altitude areas. Science of the Total Environment, 2017, 609, 446-455.	3.9	33
53	Preparation and formation process of α-MnS@MoS2 microcubes with hierarchical core/shell structure. Journal of Colloid and Interface Science, 2017, 507, 18-26.	5.0	24
54	Î-MnO <sub>2</sub> nanofiber/single-walled carbon nanotube hybrid film for all-solid-state flexible supercapacitors with high performance. Journal of Materials Chemistry A, 2017, 5, 19107-19115.	5.2	44

#	Article	IF	CITATIONS
55	Targeting Activation of CO <sub>2</sub> and H <sub>2</sub> over Ruâ€Loaded Ultrathin Layered Double Hydroxides to Achieve Efficient Photothermal CO <sub>2</sub> Methanation in Flowâ€Type System. Advanced Energy Materials, 2017, 7, 1601657.	10.2	193
56	Polyaniline Nanorods Grown on Hollow Carbon Fibers as Highâ€Performance Supercapacitor Electrodes. ChemElectroChem, 2016, 3, 1142-1149.	1.7	24
57	Telluriumâ€Assisted Epitaxial Growth of Largeâ€Area, Highly Crystalline ReS <sub>2</sub> Atomic Layers on Mica Substrate. Advanced Materials, 2016, 28, 5019-5024.	11.1	169
58	Î-MnO <sub>2</sub> /holey graphene hybrid fiber for all-solid-state supercapacitor. Journal of Materials Chemistry A, 2016, 4, 9088-9096.	5.2	101
59	20â€mmâ€Large Singleâ€Crystalline Formamidiniumâ€Perovskite Wafer for Mass Production of Integrated Photodetectors. Advanced Optical Materials, 2016, 4, 1829-1837.	3.6	316
60	High-energy asymmetric electrochemical capacitors based on oxides functionalized hollow carbon fibers electrodes. Nano Energy, 2016, 30, 9-17.	8.2	70
61	Atomic Layers: Tellurium-Assisted Epitaxial Growth of Large-Area, Highly Crystalline ReS2 Atomic Layers on Mica Substrate (Adv. Mater. 25/2016). Advanced Materials, 2016, 28, 5018-5018.	11.1	5
62	Controlled growth of large-area anisotropic ReS <sub>2</sub> atomic layer and its photodetector application. Nanoscale, 2016, 8, 18956-18962.	2.8	114
63	Optical Anisotropy of Black Phosphorus in the Visible Regime. Journal of the American Chemical Society, 2016, 138, 300-305.	6.6	273
64	Mn 3 O 4 nanocrystalline/graphene hybrid electrode with high capacitance. Electrochimica Acta, 2016, 188, 398-405.	2.6	33
65	Physical vapor deposition synthesis of two-dimensional orthorhombic SnS flakes with strong angle/temperature-dependent Raman responses. Nanoscale, 2016, 8, 2063-2070.	2.8	206
66	Formation process of holey graphene and its assembled binder-free film electrode with high volumetric capacitance. Electrochimica Acta, 2016, 187, 543-551.	2.6	94
67	Extraordinarily high-rate capability of polyaniline nanorod arrays on graphene nanomesh. Journal of Power Sources, 2016, 304, 111-118.	4.0	68
68	Hierarchically porous carbon by activation of shiitake mushroom for capacitive energy storage. Carbon, 2015, 93, 315-324.	5.4	395
69	Three-Dimensional Tubular MoS <sub>2</sub> /PANI Hybrid Electrode for High Rate Performance Supercapacitor. ACS Applied Materials & Interfaces, 2015, 7, 28294-28302.	4.0	231
70	Identifying the Crystalline Orientation of Black Phosphorus Using Angleâ€Resolved Polarized Raman Spectroscopy. Angewandte Chemie, 2015, 127, 2396-2399.	1.6	97
71	Identifying the Crystalline Orientation of Black Phosphorus Using Angleâ€Resolved Polarized Raman Spectroscopy. Angewandte Chemie - International Edition, 2015, 54, 2366-2369.	7.2	284
72	Growth of MoS <sub>2(1–<i>x</i>)</sub> Se <sub>2<i>x</i></sub> ( <i>x</i> = 0.41–1.00) Monolayer Alloys with Controlled Morphology by Physical Vapor Deposition. ACS Nano, 2015, 9, 7450-7455.	7.3	217

#	Article	IF	CITATIONS
73	Mesoporous-assembled MnO <sub>2</sub> with large specific surface area. Journal of Materials Chemistry A, 2015, 3, 14567-14572.	5.2	14
74	Nitrogenâ€Đoped Carbon Nanotube Aerogels for Highâ€Performance ORR Catalysts. Small, 2015, 11, 3903-3908.	5.2	96
75	A self-powered graphene–MoS2 hybrid phototransistor with fast response rate and high on–off ratio. Carbon, 2015, 92, 126-132.	5.4	80
76	Activation of graphene aerogel with phosphoric acid for enhanced electrocapacitive performance. Carbon, 2015, 92, 1-10.	5.4	193
77	CMP Aerogels: Ultrahighâ€5urfaceâ€Area Carbonâ€Based Monolithic Materials with Superb Sorption Performance. Advanced Materials, 2014, 26, 8053-8058.	11.1	125
78	Dynamic Response of Underground Circular Lining Tunnels Subjected to Incident P Waves. Mathematical Problems in Engineering, 2014, 2014, 1-11.	0.6	15
79	Growth of Largeâ€Area 2D MoS <sub>2(1â€<i>x</i>)</sub> Se <sub>2<i>x</i></sub> Semiconductor Alloys. Advanced Materials, 2014, 26, 2648-2653.	11.1	347
80	High Responsivity and Gate Tunable Grapheneâ€MoS <sub>2</sub> Hybrid Phototransistor. Small, 2014, 10, 2300-2306.	5.2	301
81	Observation of Low-Frequency Combination and Overtone Raman Modes in Misoriented Graphene. Journal of Physical Chemistry C, 2014, 118, 3636-3643.	1.5	15
82	Identifying sp–sp <sup>2</sup> carbon materials by Raman and infrared spectroscopies. Physical Chemistry Chemical Physics, 2014, 16, 11303-11309.	1.3	81
83	Semiconductors: Growth of Large-Area 2D MoS2(1-x ) Se2x Semiconductor Alloys (Adv. Mater. 17/2014). Advanced Materials, 2014, 26, 2763-2763.	11.1	8
84	Substrate Engineering by Hexagonal Boron Nitride/SiO <sub>2</sub> for Hysteresisâ€Free Graphene FETs and Largeâ€Scale Graphene p–n Junctions. Chemistry - an Asian Journal, 2013, 8, 2446-2452.	1.7	26
85	Investigating the Mechanism of Hysteresis Effect in Graphene Electrical Field Device Fabricated on SiO <sub>2</sub> Substrates using Raman Spectroscopy. Small, 2012, 8, 2833-2840.	5.2	120
86	Fabrication of TiO2 nanotubes with extended periodical morphology by alternating-current anodization. Electrochemistry Communications, 2012, 17, 34-37.	2.3	32
87	Effect of Graphene Fermi Level on the Raman Scattering Intensity of Molecules on Graphene. ACS Nano, 2011, 5, 5338-5344.	7.3	193
88	Expanding the photoresponse range of TiO2 nanotube arrays by CdS/CdSe/ZnS quantum dots co-modification. Journal of Photochemistry and Photobiology A: Chemistry, 2011, 224, 25-30.	2.0	49
89	Modulating the Chargeâ€Transfer Enhancement in GERS using an Electrical Field under Vacuum and an n/pâ€Doping Atmosphere. Small, 2011, 7, 2945-2952.	5.2	65
90	Can Graphene be used as a Substrate for Raman Enhancement?. Nano Letters, 2010, 10, 553-561.	4.5	914

Hua	Xu

#	Article	IF	CITATIONS
91	Shell-Controlled Photoluminescence in CdSe/CNT Nanohybrids. Nanoscale Research Letters, 2009, 4, 1146-52.	3.1	30